

In the format provided by the authors and unedited.

Photovoltaic panel cooling by atmospheric water sorption–evaporation cycle

Renyuan Li ¹, Yusuf Shi ¹, Mengchun Wu¹, Seunghyun Hong ¹ and Peng Wang ^{1,2} 

¹Water Desalination and Reuse Center, Division of Biological and Environmental Science and Engineering, King Abdullah University of Science and Technology, Thuwal, Saudi Arabia. ²Department of Civil and Environmental Engineering, The Hong Kong Polytechnic University, Hong Kong, China.
✉e-mail: peng1.wang@polyu.edu.hk

Supplementary Information:
**Photovoltaic Panel Cooling by Atmospheric Water Sorption-
Evaporation Cycle**

Renyuan Li¹, Yusuf Shi¹, Mengchun Wu¹, Seunghyun Hong¹, and Peng Wang^{1,2,*}

1. Water Desalination and Reuse Center, Division of Biological and Environmental Science and Engineering, King Abdullah University of Science and Technology, Thuwal 23955-6900, Saudi Arabia

2. Department of Civil and Environmental Engineering, The Hong Kong Polytechnic University, Hung Hom, Kowloon, Hong Kong, China

* Address correspondence to peng.wang@kaust.edu.sa; peng1.wang@polyu.edu.hk

Supplementary Figure 1. IR images of PAM-CaCl₂ and PAM-CNT-CaCl₂ hydrogel.

Supplementary Figure 2. Full data plot of STA tests.

Supplementary Figure 3. Vapor pressure difference ΔP as a function of mass fraction of CaCl₂ and ambient air temperature

Supplementary Figure 4. Schematic of water vapor transfer across a vapor phase thin film.

Supplementary Figure 5. Vapor transfer as a function of the ambient temperature and wind speed for the sorption and desorption process.

Supplementary Figure 6. Schematic of PV panel without cooling layer and with cooling layer.

Supplementary Figure 7. I-V, V_{oc} , FF, efficiency, and P_{max} of PV panel with and without the hydrogel cooling layer under 0.8 kW/m² sunlight irradiation.

Supplementary Figure 8. I-V, V_{oc} , FF, efficiency, and P_{max} of PV panel with and without the hydrogel cooling layer under 1.0 kW/m² sunlight irradiation.

Supplementary Figure 9. I-V, V_{oc} , FF, efficiency, and P_{max} of PV panel with and without the hydrogel cooling layer under 1.2 kW/m² sunlight irradiation.

Supplementary Figure 10. IV curve of PV panel with and without hydrogel cooling layer.

Supplementary Figure 11. Experimental setup of PV panel cooling test in outdoor condition in Mid-August of 2019.

Supplementary Figure 12. Water vapor sorption curve of the hydrogel. Temperature and humidity between 18:00, August 13 and 9:00, Aug. 14.

Supplementary Figure 13. Sunlight strength, overall solar irradiance, relative humidity and ambient temperature of August 14 and August 15, 2019. Power and surface temperature of PV panel. Accumulated electricity generated on August 14 and August 15.

Supplementary Figure 14. Experimental setup of PV panel cooling test in outdoor condition in early-December, 2019.

Supplementary Figure 15. Sunlight strength curve of November 30, December 01, December 4, and December 5, 2019. Overall solar irradiance of the two individual outdoor test. Weight change curve of the hydrogel cooling layer during the test. PV panel temperature during the test. The power of PV panel. Accumulated electricity generated during the test observed from the two modes.

Supplementary Figure 16. Temperature and relative humidity of November 30-December 2, December 4-5.

Supplementary Figure 17. Schematic of outdoor test PV-hydrogel system.

Supplementary Figure 18. Solar irradiation during stability test. The ambient condition during the stability test. The temperature of PV panel and the weight change curve of the hydrogel

cooling layer. The power of PV panel during operation and the accumulated electricity generated in daily base.

Supplementary Table 1. Parameters used for the calculation of mass transfer across the hydrogel-air interface.

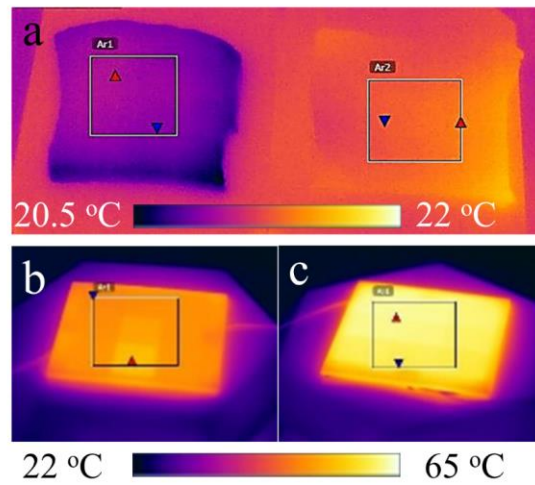
Supplementary Table 2. V_{oc} , FF, Efficiency (%) and P_{max} of PV panel at $t=90$ min and $t=180$ min.

Supplementary Table 3. Parameters of simulated daylight test.

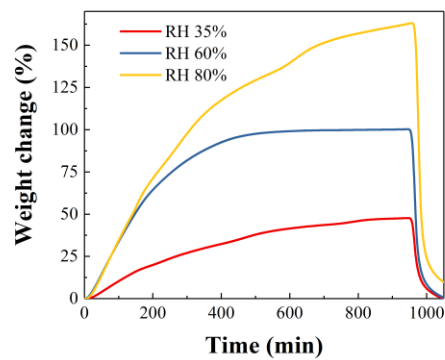
Supplementary note 1. Theoretical model

Supplementary note 2. PV cooling performance test in real outdoor conditions.

Supplementary note 3. Recent publications on AWH cooling concept on other journals



Supplementary Figure 1. (a) IR images of PAM-CaCl₂ (left) and PAM-CNT-CaCl₂ hydrogel (right). The comparison indicates a lower emissivity of PAM-CaCl₂ hydrogel. Both hydrogels were pre-stabilized under the same conditions for 1 hour. (b) and (c) IR images of PV panel with and without hydrogel attached, respectively.



Supplementary Figure 2. Full data plot of STA tests. The curves contain both sorption and desorption process of the hydrogel. In doing the desorption measurement, the temperature of STA furnace was first increased from 25 to 85 °C with a ramp of 10 °C/min, and kept at 85 °C for 90 min. The humidity of the purged nitrogen flow was adjusted to RH 15% during desorption test.

Supplementary note 1. Theoretical model

Physical and chemical processes of water vapor sorption-desorption

Theoretically, water vapor sorption by CaCl_2 takes place in two stages, i.e. hydration and deliquescence of CaCl_2 . While the evaporation/desorption of the sorbed water is driven by the heat from PV panel during daytime.

Stage 1: hydration

Reaction formula	ΔrH_m (kJ/mol)
$\text{CaCl}_2 + \text{H}_2\text{O} \rightarrow \text{CaCl}_2 \cdot \text{H}_2\text{O}$	-315.4
$\text{CaCl}_2 \cdot \text{H}_2\text{O} + \text{H}_2\text{O} \rightarrow \text{CaCl}_2 \cdot 2\text{H}_2\text{O}$	-293.3
$\text{CaCl}_2 \cdot 2\text{H}_2\text{O} + 2\text{H}_2\text{O} \rightarrow \text{CaCl}_2 \cdot 4\text{H}_2\text{O}$	-605.5
$\text{CaCl}_2 \cdot 4\text{H}_2\text{O} + 2\text{H}_2\text{O} \rightarrow \text{CaCl}_2 \cdot 6\text{H}_2\text{O}$	-598.2
Total ΔrH_m (KJ/mol)	-1812.4

(ΔrH_m is calculated based on the formation heat of the referred components.¹⁾)

In this stage, CaCl_2 crystal absorbs water molecules via hydration reaction and forms hydrates. After $\text{CaCl}_2 \cdot 6\text{H}_2\text{O}$ is formed, further water vapor capture is moved to the 2nd stage, namely deliquescence of CaCl_2 .

Stage 2: deliquescence

In the course of deliquescence, CaCl_2 further sorbs moisture beyond its hydration water. The solid salt gradually dissolves in the sorbed water and forms a solution. The driving force of water vapor sorption by the deliquescing salt solution is the water vapor pressure difference between the water in the salt solution and that in the atmosphere. As more water vapor is being sorbed by the solution, the driving force decreases. Thus, the salt deliquescence can be thought of as dilution of a concentrated CaCl_2 water solution by atmospheric water. The macroscopic water vapor sorption stops when the vapor pressure of the salt solution is equal to that in the atmosphere where a sorption equilibrium is reached.

Stage 3: water desorption by evaporation

During daytime, the heat from PV panel drives evaporation of the sorbed water out of the CaCl_2 solution obtained in Stage 2. The driving force for water removal by evaporation is the higher water vapor pressure of the CaCl_2 solution under elevated temperatures than that of the atmosphere. Water evaporation is endothermic and thus removes heat along with the evaporated water molecules. As water is being continuously removed out, the solution concentration increases and its vapor pressure decreases accordingly, leading to a gradually diminishing driving force. The water evaporation ceases when the driving force becomes zero.

Please be noted that a full-dehydration of CaCl_2 solution requires temperature higher than 142 °C, which is unachievable by PV heat.^{2,3} The temperature of PV-hydrogel cooling layer reaches no more than 60 °C in this project, which is far from being adequate to remove crystal hydration water out of CaCl_2 . As a result, the term “original weight” of the hydrogel cooling layer in the

manuscript is actually the weight of polyacrylamide, CaCl₂ along with its non-removable crystallized water and 10 wt.% of residual liquid water, which is unable to be evaporated.

Theoretical models

1. Driving force of water vapor sorption and desorption

The driving force for the water vapor sorption/desorption process is the difference of the water vapor pressure between the CaCl₂ solution in the surface of hydrogel and the surrounding air. The vapor pressure difference (ΔP , mmHg) can be calculated by equation (S1).³

$$\Delta P = \chi_{H_2O} \cdot P_s - P_a \quad (S1)$$

Where χ_{H_2O} is molar fraction of water in CaCl₂ solution, P_s is saturated water vapor pressure (mmHg) at the temperature of CaCl₂ solution (T_s , °C) right at the surface of hydrogel, and P_a is partial pressure (mmHg) of water vapor in the ambient air with the temperature of T (°C), which is calculated by equation (S2).

$$P_a = P \times RH \quad (S2)$$

Where RH is the relative humidity and P is saturated water vapor pressure (mmHg) at the temperature of T , which can be calculated via Antoine's equation:

$$\log_{10} P = A - \frac{B}{C+T} \quad (S3)$$

Thus,

$$P = 10^{(A - \frac{B}{C+T})} \text{ and } P_s = 10^{(A - \frac{B}{C+T_s})} \quad (S4)$$

Where A, B and C are constant, equal to 8.07, 1730.63, and 233.43, respectively.

χ_{H_2O} is calculated by equations (S5-S7).

$$\chi_{H_2O} = \frac{n_{H_2O}}{n_{H_2O} + N_{ion} \cdot n_{CaCl_2}} \quad (S5)$$

$$n_{H_2O} = \frac{m \cdot (1 - F_{CaCl_2})}{M_{H_2O}} \quad (S6)$$

$$n_{CaCl_2} = \frac{m \cdot F_{CaCl_2}}{M_{CaCl_2}} \quad (S7)$$

Where n_{H_2O} and n_{CaCl_2} are moles of water and CaCl₂ in the solution, respectively, m is total mass of CaCl₂ solution, M_{CaCl_2} is molar mass of CaCl₂, M_{H_2O} is molar mass of water, F_{CaCl_2} is mass fraction of CaCl₂ in the solution, and N_{ion} is 3 for CaCl₂.

Therefore, ΔP can be derived into equation (S8) and (S9).

$$\Delta P = \frac{n_{H_2O}}{n_{H_2O} + N_{ion} \cdot n_{CaCl_2}} \cdot 10^{(A - \frac{B}{C+T_s})} - 10^{(A - \frac{B}{C+T})} \times RH \quad (S8)$$

$$\Delta P = \frac{\frac{(1-F_{CaCl_2})}{18}}{\frac{(1-F_{CaCl_2})}{18} + 3 \cdot \frac{F_{CaCl_2}}{111}} \cdot 10^{\left(8.07 - \frac{1730.63}{233.43+T_s}\right)} - 10^{\left(8.07 - \frac{1730.63}{233.43+T}\right)} \times RH \quad (S9)$$

Due to the very high salt concentration in the solution, the colligative properties of solution are inaccurate to reflect the real vapor pressure of the solution. Thereby, a calibration function $F(F_{CaCl_2})$ is established by comparing the difference between the calculated vapor pressure and actual vapor pressure under different temperature and salt mass fraction.

$$F(F_{CaCl_2}) = -1.56 \cdot F_{CaCl_2} + 0.42575 \cdot F_{CaCl_2}^2 + 1.1018 \quad (S10)$$

Thereby, equation (R8) and (R9) are transformed into:

$$\Delta P = F(F_{CaCl_2}) \cdot \frac{n_{H_2O}}{n_{H_2O} + N_{ion} \cdot n_{CaCl_2}} \cdot 10^{\left(A - \frac{B}{C+T_s}\right)} - 10^{\left(A - \frac{B}{C+T}\right)} \times RH \quad (S11)$$

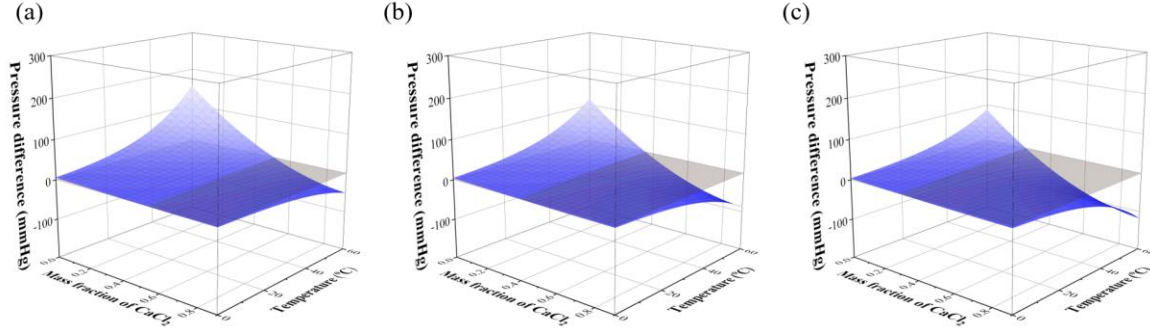
$$\Delta P = F(F_{CaCl_2}) \cdot \frac{\frac{(1-F_{CaCl_2})}{18}}{\frac{(1-F_{CaCl_2})}{18} + 3 \cdot \frac{F_{CaCl_2}}{111}} \cdot 10^{\left(8.07 - \frac{1730.63}{233.43+T_s}\right)} - 10^{\left(8.07 - \frac{1730.63}{233.43+T}\right)} \times RH \quad (S12)$$

During daytime, the temperature of the hydrogel surface (T_s) is higher than the temperature of the surrounding air (T) due to photothermal heat generation by PV panel. The temperature difference at the ambient air-hydrogel interface is usually several degree Celsius, and it varies depending on ambient conditions, salt solution concentration in the hydrogel, sunlight strength, etc. To reasonably simplify the calculation, it is assumed $T_s - T = 5$ °C. Supplementary Figure 3 shows the relationships among ΔP , T , and F_{CaCl_2} under ambient RH of 35%, 60%, and 80%, respectively.

In these figures, $\Delta P < 0$ indicates water vapor sorption process while $\Delta P > 0$ indicates water evaporation/desorption process and $\Delta P = 0$ denotes an equilibrium state. These figures delineate the working conditions for the hydrogel cooling layer, and point out conditions at which the hydrogel captures or releases water vapor.

As can be seen, the vapor sorption by the cooling layer is highly dependent on the ambient humidity, with higher ambient humidity leading to higher vapor sorption. The mass fraction of $CaCl_2$ in the solution (i.e., the concentration of $CaCl_2$) determines the driving force of water vapor sorption, and the minimum mass fraction of $CaCl_2$ required to drive vapor sorption decreases with increasing ambient humidity.

During the desorption process (i.e., $\Delta P > 0$), the pressure difference decreases along with the evaporation of $CaCl_2$ solution (i.e., mass fraction of $CaCl_2$ increases), and thus the evaporation rate will drop if the ambient temperature remains unchanged, leading to a deducted heat removal rate of the hydrogel.



Supplementary Figure 3. Vapor pressure difference ΔP as a function of mass fraction of CaCl_2 and ambient air temperature at (a) RH 35%, (b) RH 60%, (c) RH 80%.

2. Mass transfer

A mass transfer model is established to simulate the water vapor sorption/desorption dynamics. Given the fact that the hydrogel has a residual water mass of ~ 10 wt.% after water removal under the conditions of this project, we consider the cooling layer as a nonporous bulk-phased material.

Vapor phase thin film⁴ model is used to simulate mass transfer of vapor across the hydrogel-air interface (Supplementary Figure 4) and to determine water vapor flux across the interface. In this model, a thin film of vapor phase is assumed to be at the hydrogel-air interface and a linear water vapor concentration profile is assumed across the thickness of the thin film, which is dependent on both the diffusion coefficient of water vapor at specific conditions and the air flow condition. Given the regular ambient wind velocity and dimension of PV panel, a laminar boundary layer is assumed for the vapor phase thin film. The mass transfer of water vapor across the boundary layer can be expressed by Fick's Law as equation (S13).⁵

$$j_v = -D_v \cdot \frac{dc}{dl} = \frac{D_v}{l} \cdot (c_i - c_a) \quad (\text{S13})$$

Where j_v is mole flux of water vapor ($\text{mol}/(\text{m}^2 \cdot \text{s})$), D_v is diffusion coefficient of water vapor in air (m^2/s), c is concentration of water vapor (mol/m^3), l is diffusion length (*i.e.* thickness of the vapor phase thin film) (m), c_i and c_a are water vapor concentration in the hydrogel-air interface and the bulk ambient air flow (mol/m^3). The number of moles of water vapor transferred (N_v) can then be calculated by equation (S14).

$$\frac{dN_v}{dt} = j_v \cdot A = \frac{D_v}{l} \cdot (c_i - c_a) \cdot A \quad (\text{S14})$$

Where t is time and A is surface area of hydrogel (m^2). c_a and c_i can be calculated by the ideal gas law as shown in equations (S15) and (S16).

$$c_a = \frac{P_a \times 133.32}{R(T+273.15)} \quad (\text{S15})$$

$$c_i = \frac{P_i \times 133.32}{R(T_s+273.15)} = \frac{\chi_{H_2O} \cdot P_s \times 133.32}{R(T_s+273.15)} \quad (\text{S16})$$

Where P_a is partial pressure of water vapor in ambient air (mmHg), P_i is water vapor pressure at hydrogel surface (mmHg), χ_{H_2O} is the molar fraction of water, P_s is the saturated water vapor pressure (mmHg) at temperature T_s , R is gas constant, and T and T_s are the temperature of air and hydrogel ($^{\circ}C$), respectively. (1 mmHg=133.32 Pascal)

The molar fraction of water χ_{H_2O} varies at different stage of water vapor sorption and desorption and is obtained experimentally.

The diffusion length, l , can be calculated based on laminar boundary layer theory. For laminar flow over a square-shaped flat plate, the diffusion length is calculated by equation (S17):

$$l = \frac{\sqrt{A}}{0.646 \cdot \left(\frac{U\sqrt{A}}{v}\right)^{1/2} \cdot \left(\frac{v}{D_v}\right)^{1/3}} \quad (S17)$$

Where U and v are velocity (m/s) and viscosity (m^2/s) of air.

Then equation (S14) can be transformed to equation (S18).

$$\frac{dN_v}{dt} = \frac{D_v}{l} \cdot (c_i - c_a) \cdot A = \frac{D_v \cdot 0.646 \cdot \left(\frac{U\sqrt{A}}{v}\right)^{1/2} \cdot \left(\frac{v}{D_v}\right)^{1/3}}{\sqrt{A}} \cdot \left(\frac{\chi_{H_2O} \cdot P_s \times 133.32}{R(T_s + 273.15)} - \frac{P_a \times 133.32}{R(T + 273.15)}\right) \cdot A \quad (S18)$$

The equation (S18) can be further transformed to equation (S19) and calibrated by equation (S10):

$$\frac{d_m}{d_t} = \frac{D_v \cdot 0.646 \cdot \left(\frac{U\sqrt{A}}{v}\right)^{1/2} \cdot \left(\frac{v}{D_v}\right)^{1/3}}{\sqrt{A}} \cdot \left(\frac{\frac{(1-F_{CaCl_2})}{M_{H_2O}}}{\frac{(1-F_{CaCl_2})}{M_{H_2O}} + N_{ion} \cdot \frac{F_{CaCl_2}}{M_{CaCl_2}}} \cdot 10^{\left(8.07 - \frac{1730.63}{233.43 + T_s}\right)} \times F(F_{CaCl_2}) - \frac{RH \cdot 10^{\left(8.07 - \frac{1730.63}{233.43 + T}\right)}}{R(T + 273.15)}\right) \cdot 133.32 \cdot A \cdot M_{H_2O} \quad (S19)$$

Where M_{H_2O} , M_{CaCl_2} , and F_{CaCl_2} are molar mass of water, molar mass of $CaCl_2$, and mass fraction of $CaCl_2$ in the $CaCl_2$ solution, respectively. N_{ion} is 3 for $CaCl_2$.

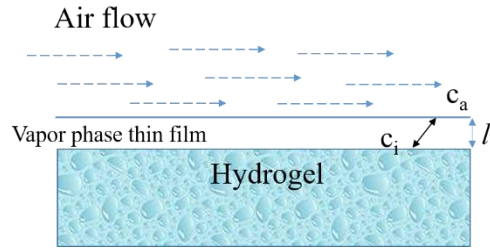
$$\frac{d_m}{d_t} = \frac{D_v \cdot 0.646 \cdot \left(\frac{U\sqrt{A}}{v}\right)^{1/2} \cdot \left(\frac{v}{D_v}\right)^{1/3}}{\sqrt{A}} \cdot \left(\frac{\frac{(1-F_{CaCl_2})}{18}}{\frac{(1-F_{CaCl_2})}{18} + 3 \cdot \frac{F_{CaCl_2}}{111}} \cdot 10^{\left(8.07 - \frac{1730.63}{233.43 + T_s}\right)} \times F(F_{CaCl_2}) - \frac{RH \cdot 10^{\left(8.07 - \frac{1730.63}{233.43 + T}\right)}}{R(T + 273.15)}\right) \cdot 133.32 \cdot A \cdot 18 \quad (S20)$$

Equation (S19) and (S20) denote the capability of water vapor mass transfer as related to ambient airflow. To simplify the calculation, averaged χ_{H_2O} and F_{CaCl_2} are used to characterize the sorption process while the mass fraction of $CaCl_2$ at sorption-desorption equilibrium point is used to characterize the desorption process.

$$\chi_{H_2O} = \frac{\chi_{H_2O, equilibrium} - \chi_{H_2O, initial}}{2} + \chi_{H_2O, initial} \quad (S21)$$

$$F_{CaCl_2} = \frac{F_{CaCl_2, initial} - F_{CaCl_2, equilibrium}}{2} + F_{CaCl_2, equilibrium} \quad (S22)$$

Where the subscripts “equilibrium” and “initial” indicate the mole concentration of water or the mass fraction of $CaCl_2$ at the equilibrium and initial state (the time when the water vapor sorption/desorption starts), respectively.



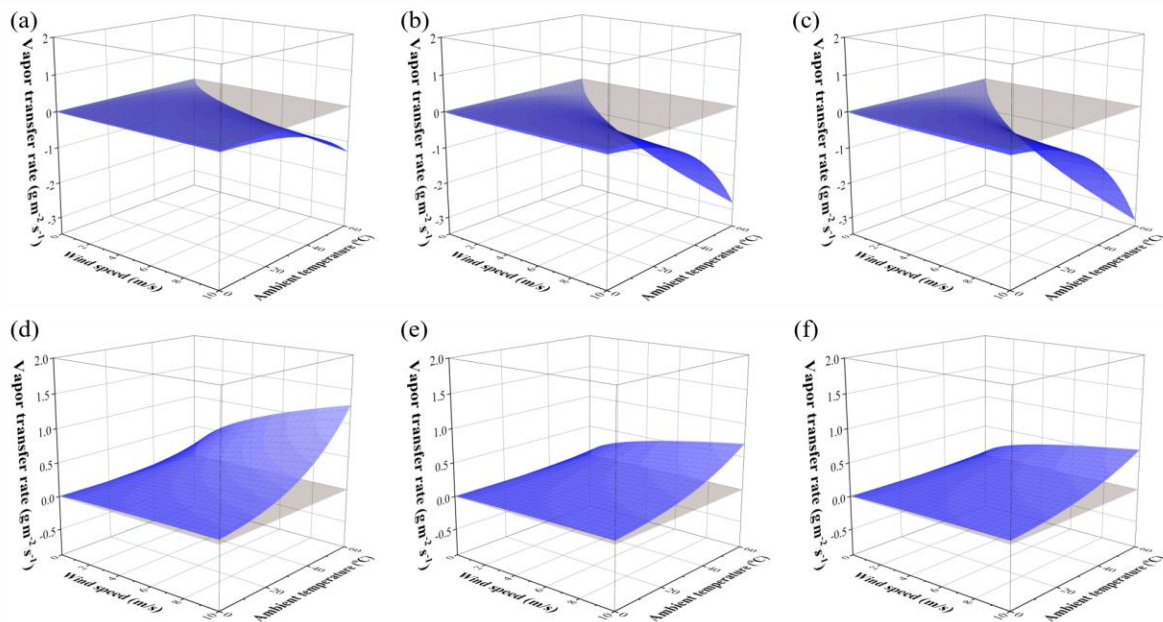
Supplementary Figure 4. Schematic of water vapor transfer across a vapor phase thin film.

Supplementary Table 1 lists essential parameters needed for conducting calculation. The calculated results are plotted in Supplementary Figure 5.

Supplementary Table 1. Parameters used for the calculation of mass transfer across the hydrogel-air interface^{6,7}

RH	F_{CaCl_2} equilibrium	F_{CaCl_2} initial	F_{CaCl_2}	v m^2/s	A m^2	D_v m^2/s	U m/s	R $J/(mol \cdot K)$	M_{H_2O} g/mol
35 %	42.5%	85%	63.7%	1.51×10^{-5}	1.44×10^{-3}	2.82×10^{-5}	1-10	8.314	18
60 %	31.6%		58.3%						
80 %	22%		53.5%						

Note: $T_s - T = 5 \text{ }^\circ\text{C}$ is assumed in conducting calculation for vapor desorption.



Supplementary Figure 5. Vapor transfer as a function of the ambient temperature and wind speed for the sorption (a-c) and desorption process (d-e), at RH of (a)/(d) 35%, (b)/(e) 60%, (c)/(f) 80%. The shadowed plane indicates the zero plane.

As can be seen here, the vapor transfer is highly related to the ambient temperature and the wind speed. During vapor absorption by the cooling layer, a higher ambient humidity can facilitate the water vapor transfer rate. However, when the humidity is high, the evaporation-based mass transport will be inhibited, as high ambient humidity reduces the vapor pressure difference. In both sorption and desorption condition, the modeling results also show that an increase in ambient wind flow facilitates the mass transfer across the hydrogel-air interface. However, the overall performance should take into consideration the mass transfer properties within the hydrogel as well.

3. Heat transfer.

Supplementary Figure 6 compares the two primary heat transfer schemes in this work, namely, PV panel with and without cooling layer.

(a) PV panel without cooling layer. In this mode, heat dissipation is mainly by heat convection and thermal radiation. Due to the low heat conductivity of air, the contribution of heat dissipation through heat conduction is insignificant and thus conduction heat transfer is not considered in calculation.

$$\Phi_{conv} = hA(T_1 - T_{amb}) \quad (S23)$$

$$\Phi_{rad} = \sigma \varepsilon A(T_1^4 - T_{amb}^4) \quad (S24)$$

Where ϕ_{conv} and ϕ_{rad} are heat dissipation flux contributed by convective and radiative heat transfer (W). T_1 and T_{amb} are temperature of PV panel and the ambient. A is surface area (m^2), h is convective heat transfer coefficient (i.e., 5-10 for natural wind flow) ($W/(m^2 \cdot K)$), σ is Stefan-Boltzmann Constant ($5.67 \times 10^{-8} W/(m^2 \cdot K^4)$), and ε is emissivity coefficient of the PV panel.

(b) PV panel with hydrogel cooling layer. In this mode, heat dissipation is mainly by convection, radiation, and water evaporation.

$$\Phi_{conv} = hA(T_1 - T_{amb}) \quad (S25)$$

$$\Phi_{rad} = \sigma \varepsilon A(T_1^4 - T_{amb}^4) \quad (S26)$$

$$\Phi_{evap} = m \cdot (h_{lv} + h_d) \quad (S27)$$

Where ϕ_{evap} is heat dissipation flux by evaporation and m is water released from the hydrogel. h_{lv} is enthalpy of vaporization of pure water (2382 J/g at 50 °C), and h_d is differential enthalpy of dilution (J/g). The differential enthalpy of dilution can be calculated with the following equations:⁹

$$h_d = h_{d,0} \cdot \left[1 + \left(\frac{\zeta}{0.855}\right)^{1.965}\right]^{2.265} \quad (S28)$$

$$\zeta = \frac{F_{CaCl_2}}{0.8 - F_{CaCl_2}} \quad (S29)$$

$$h_{d,0} = -955.69 + 3011.97 \cdot \left(\frac{T}{228} - 1\right) \quad (S30)$$

Where $h_{d,0}$ is the reference value related to the absolute temperature T . ζ is obtained from the mass fraction of CaCl_2 (F_{CaCl_2}). Considering the energy conversion efficiency of PV panel, electricity loss due to internal resistance, 80% of the absorbed light by PV panel is assumed to be converted into heat (i.e., light-to-heat conversion efficiency η is 80%). Thus, the energy balance can be established:¹⁰

$$A \cdot P \cdot \eta \cdot t = Q_i = mC_p(T_1 - T_{amb}) + Q_{ext} \quad (\text{S31})$$

Where P is solar irradiation absorbed by PV panel (W), Q_i and Q_{ext} are the heat energy gained by PV panel and dissipated to the ambient (J). m (g) and C_p (J/K) are the mass and heat capacity of PV panel, t is time. P is calculated by equation (S32).

$$P = P_{in} \cdot A_\lambda \quad (\text{S32})$$

Where P_{in} is the incident sunlight strength, A_λ is the light absorbance of PV panel. The relationship between the total heat dissipation flux (ϕ) and Q_{ext} can be expressed by equation (S33).

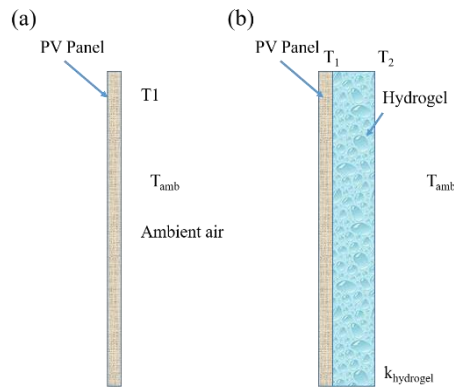
$$Q_{ext} = \phi \cdot t \quad (\text{S33})$$

For PV panel without cooling layer,

$$A \cdot P_{in} \cdot A_\lambda \cdot \eta \cdot t = mC_p(T_1 - T_{amb}) + t[\Phi_{conv} + \Phi_{rad}] \quad (\text{S34})$$

For PV panel with cooling layer,

$$A \cdot P_{in} \cdot A_\lambda \cdot \eta \cdot t = mC_p(T_1 - T_{amb}) + t[\Phi_{conv} + \Phi_{rad} + \Phi_{evap}] \quad (\text{S35})$$



Supplementary Figure 6. Schematic of PV panel (a) without cooling layer and (b) with cooling layer.

Since a variety of factors such as wind speed, ambient conditions, PV panel properties, light strength, device configurations, influence the heat transfer, it is hard to precisely calculate some numerical results through simulation. However, the heat transfer model presented here can be

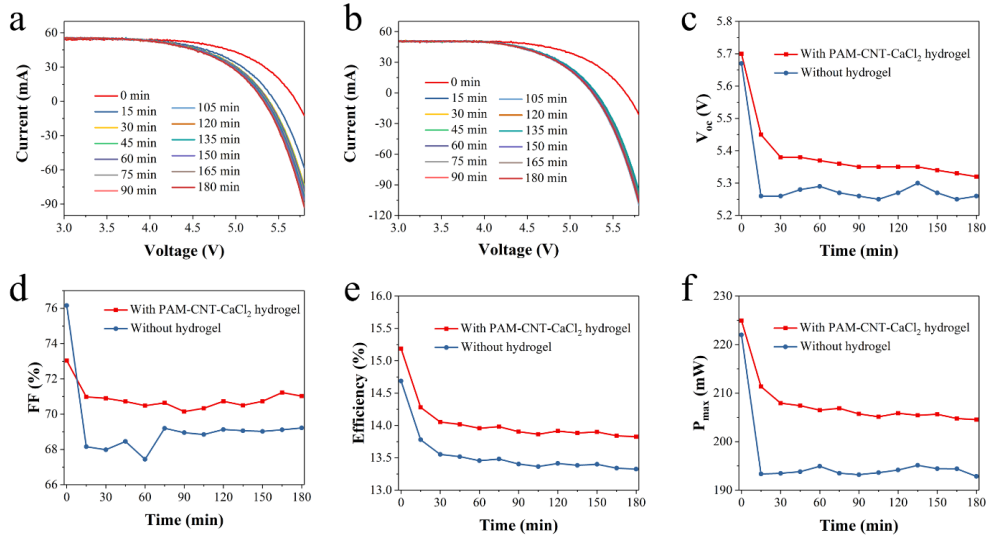
used to qualitatively propose the possible optimization direction of this cooling layer design. For example, the above heat transfer model suggest that the heat dissipation could be improved by (1) increasing the thermal conductivity of cooling layer; (2) increasing the emissivity of cooling layer to enhance radiation heat dissipation; (3) improving the system design to facilitate evaporation and improving convection heat transfer.

To end, as the summary of the theoretical work, the following conclusions are obtained regarding the limitation and the optimization directions:

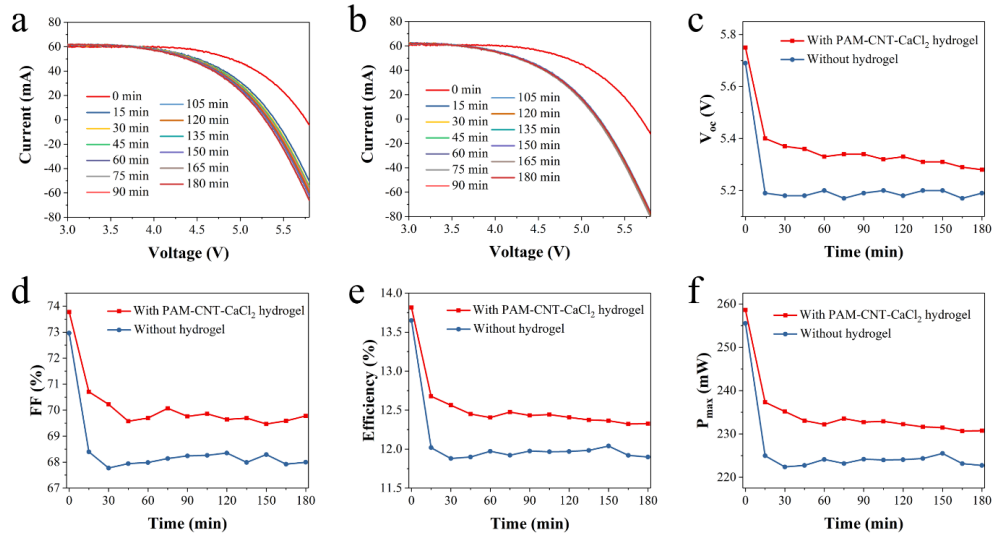
(1) The modeling results show that the sorption window for the material used in this work is a little bit narrow in low humidity condition. Thus, sorbent materials with greater sorption window can be explored. However, one has to be cautious that such a sorbent necessitates a higher temperature for desorption and thus leads to a deduction of the cooling performance.

(2) Based on the mass transfer models, water vapor mass transfer across the hydrogel-air interface can be enhanced by tuning ambient wind speed and temperature. However, the slow water transport rate within the hydrogel is the limiting factor for the whole system, which leads to a longer time required to reach sorption equilibrium and limits the maximum water uptake capacity during nighttime. The further improvement could be focused on investigating new sorption bed design or new sorbents with superior water transport. Hosting sorbents within macroporous substrates deserves future research attention.

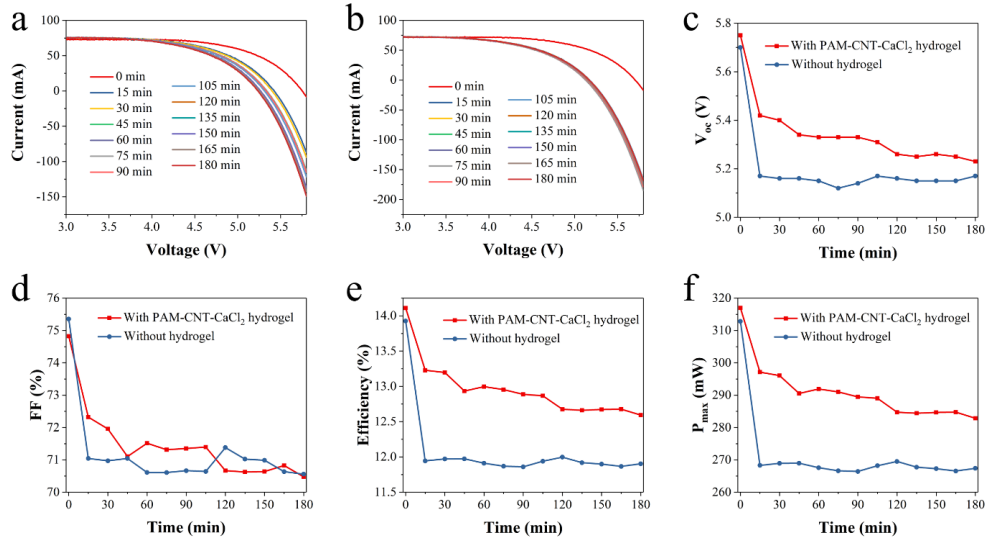
(3) Based on the heat transfer model, increasing emissivity of cooling material can further increase the cooling performance through thermal radiation. In the meanwhile, proper increase of heat conductivity of the cooling layer, for example, via using macroporous substrates with high thermal conductivity will further enhance the cooling performance.



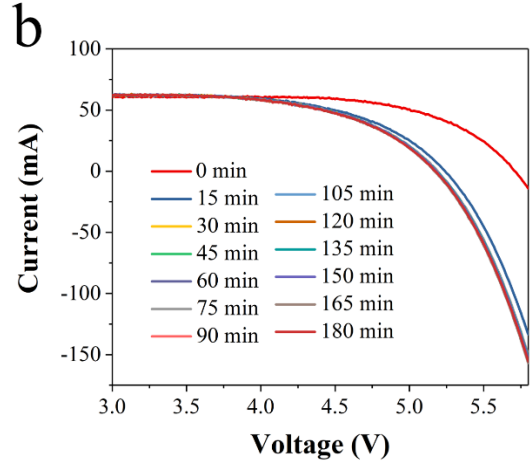
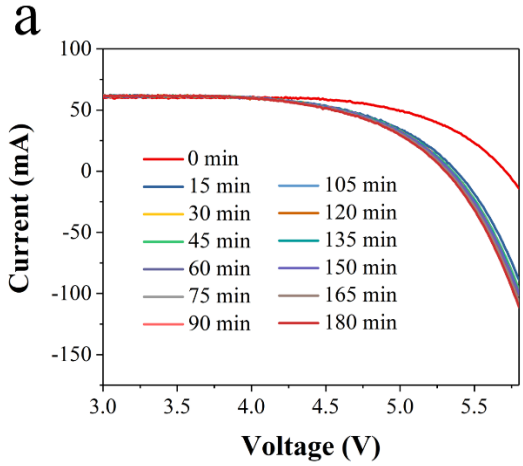
Supplementary Figure 7. I-V curves of PV panel (a) with and (b) without hydrogel cooling layer. (c) V_{oc} , (d) FF, (e) efficiency, and (f) P_{max} of PV panel with and without the hydrogel cooling layer under 0.8 kW/m^2 sunlight irradiation.



Supplementary Figure 8. (a) I-V curve of PV panel with hydrogel cooling layer attached. (b) IV curve of PV panel without hydrogel cooling layer. (c)-(f) Comparison of V_{oc} , FF, efficiency, and P_{max} , respectively. The light strength is 1.0 kW/m^2 .



Supplementary Figure 9. (a) I-V curve of PV panel with hydrogel cooling layer attached. (b) IV curve of PV panel without hydrogel cooling layer. (c)-(f) Comparison of V_{oc} , FF, efficiency, and P_{max} , respectively. The light strength is 1.2 kW/m^2 .



Supplementary Figure 10. IV curve of PV panel (a) with and (b) without hydrogel cooling layer attached.

Supplementary Table 2. V_{oc} , FF, Efficiency (%) and P_{max} of PV panel at $t=90$ min and $t=180$ min

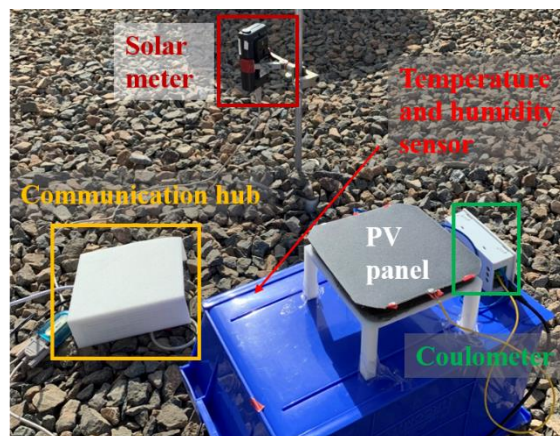
T=90 min				
	V_{oc} (V)	FF (%)	Efficiency (%)	P_{max} (mW)
Solar irradiation: 0.8 kW/m ²				
With cooling layer	5.35	70	13.9	206
Without cooling layer	5.26	69	13.5	193
Solar irradiation: 1.0 kW/m ²				
With cooling layer	5.34	70	12.4	233
Without cooling layer	5.19	68	11.8	225
Solar irradiation: 1.2 kW/m ²				
With cooling layer	5.33	71	12.8	289
Without cooling layer	5.14	70	11.9	270
T=180 min				
	V_{oc} (V)	FF (%)	Efficiency (%)	P_{max} (mW)
Solar irradiation 0.8 kW/m ²				
With cooling layer	5.32	71	14.0	205
Without cooling layer	5.26	69	13.5	193
Solar irradiation: 1.0 kW/m ²				
With cooling layer	5.28	70	12.6	231
Without cooling layer	5.19	68	11.8	225
Solar irradiation: 1.2 kW/m ²				
With cooling layer	5.23	70	12.8	283
Without cooling layer	5.17	70	11.9	267

Supplementary note 2. PV cooling performance test in real outdoor conditions.

Outdoor field test in summer

The first outdoor test was conducted in mid-August (summer) of 2019 when the manuscript was under review. The second outdoor test was conducted in the early December (winter) of 2019. Both experiments were performed at KAUST campus.

The experiment setup of the summer outdoor test is shown as a photo in Supplementary Figure 11:

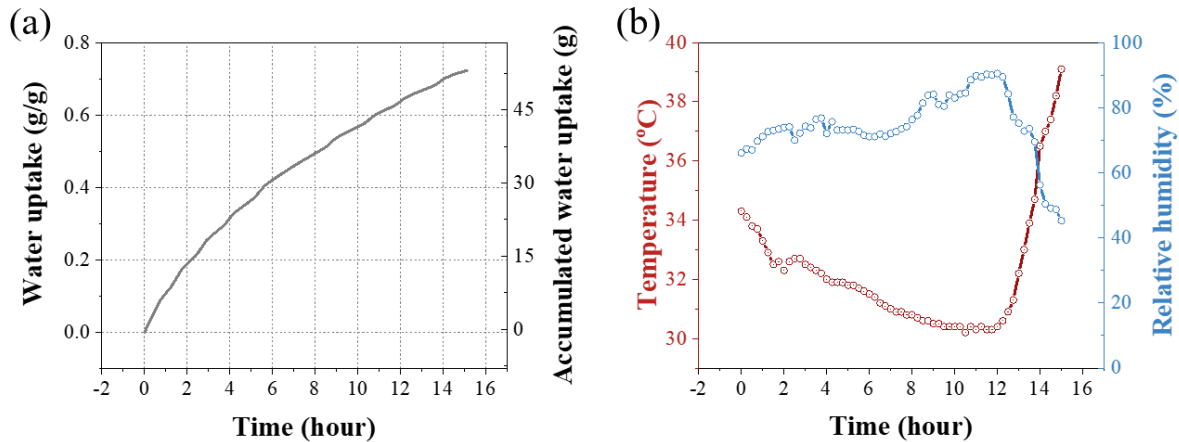


Supplementary Figure 11. Experimental setup of PV panel cooling test in outdoor condition in mid-August of 2019.

In more details, the PV panel was horizontally placed on the top of house roof in KAUST campus. The solar meter was used to record the sunlight strength during the test and temperature and humidity sensor inside the blue box were used to record the weather condition. A rectangular opening notch was cut on four sidewalls of the box to ensure the weather condition inside the blue box was consistent with the surrounding ambient. A coulometer was employed to real-time monitor the PV panel and record its electricity generation. All of these measuring tools were connected to a computer via a communication hub. The dimension of the commercialized PV panel for the outdoor test was $12 \times 12 \text{ cm}^2$, and a hydrogel with same dimension and a thickness of $\sim 0.8 \text{ cm}$ was attached on the backside of the PV panel.

The dry weight of the hydrogel (i.e. the weight of polyacrylamide and CaCl_2 along with its non-removable crystallized water) was $\sim 65 \text{ g}$. Prior to the test, the system was first exposed to ambient for one night to sorb water vapor and then exposed to the sunlight for one day to release the sorbed water to condition the hydrogel to the real outdoor condition. After the conditioning operation, with the hydrogel with the original weight of $\sim 73 \text{ g}$ (i.e. the weight of polyacrylamide, CaCl_2 , and residual water) was obtained.

Water vapor sorption test was started in the evening of August 13 at 18:00 of the day (set as 0 hour) and ended on August 14 at 9:00 am. The water vapor sorption curve along with the temperature/humidity curves are displayed in Supplementary Figure 12. Both water uptake and accumulated water uptake values were calculated based on the original weight of hydrogel.



Supplementary Figure 12. (a) Water vapor sorption curve of the hydrogel. (b) Temperature and humidity between 18:00, August 13 and 9:00, Aug. 14. The original weight of the hydrogel prior water vapor sorption was 73 g.

The water uptake rate and the accumulated amount of water absorbed by the hydrogel in the outdoor field test was lower than the STA mode largely due to the much larger hydrogel size.

To ensure a higher cooling performance and ensure the appropriate amount of water absorbed during the sorption process, we chose to use two identical pieces of hydrogel with thinner dimension instead of one thick hydrogel in the outdoor test. As can be seen from Supplementary Figure 14a, after 15 hours of water vapor sorption process during the night, ~51 g of water was absorbed. The replacement of hydrogel during the PV cooling test was conducted in the middle of the daytime test (i.e., 13:00).

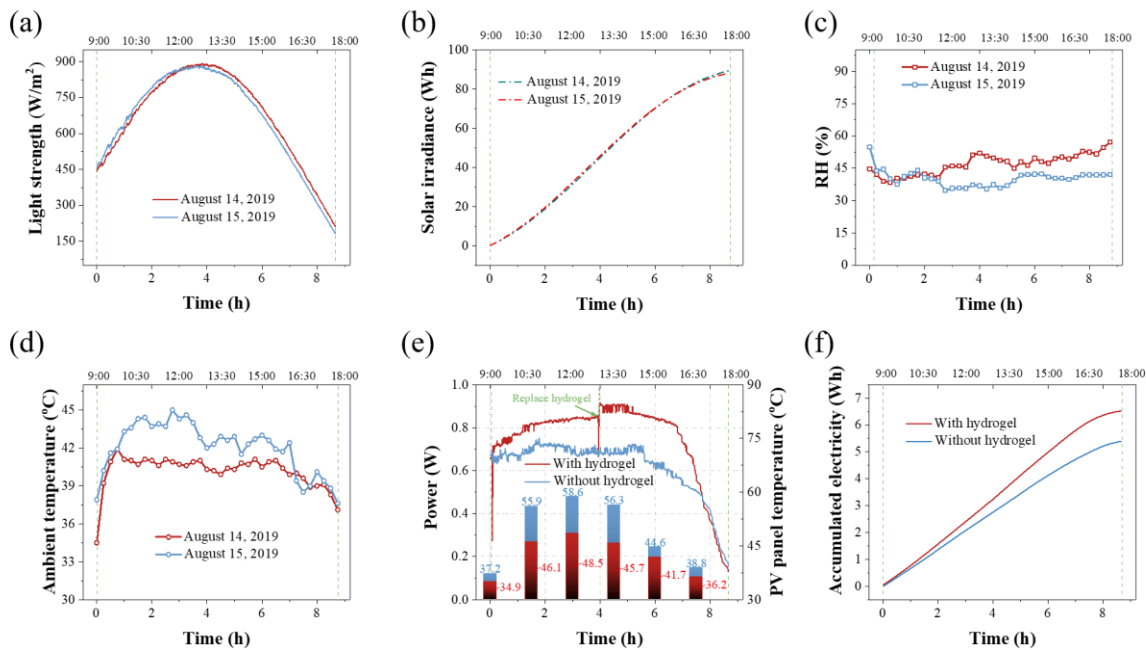
The experimental results are shown in Supplementary Figure 13. The time-dependent sunlight strength (Supplementary Figure 13a), the overall sunlight irradiance (Supplementary Figure 13b), and the relative humidity (Supplementary Figure 13c) of August 14 and 15 were quite close, while the ambient temperature (Supplementary Figure 13d) of August 15 was slightly higher than August 14. The outdoor tests of PV panels with hydrogel and without hydrogel were conducted in parallel on August 14 and 15, respectively.

The surface temperature of the PV panel was recorded every 90 minutes with an IR camera and their values are displayed as the histogram of Supplementary Figure 13e. As can be seen, a distinctive temperature difference between the PV panels with hydrogel and without hydrogel could be observed especially within the period between 10:30-15:00. A maximum of 10.6 °C difference was achieved at 13:30. A clear power enhancement could be observed after the PV panel was attached with hydrogel cooling layer.

An interesting phenomenon could be observed when the test was about to end (i.e. after 16:30 pm) where the power of the cooled PV panel was slightly lower than that of PV panel without cooling layer. The sunlight strength after 16:30 was less than 400 W/m². The heat generated from the PV panel was significantly reduced and the concentration of the salt solution inside hydrogel was increased due to the evaporation. Thus, the generated heat may not be enough to

maintain the evaporation process, and the cooling layer indeed was inhibitory to the heat dissipation from the PV panel. In this case, the temperature of the PV panel with cooling layer attached was slightly higher than the one without cooling layer, demonstrating a slightly degraded power output.

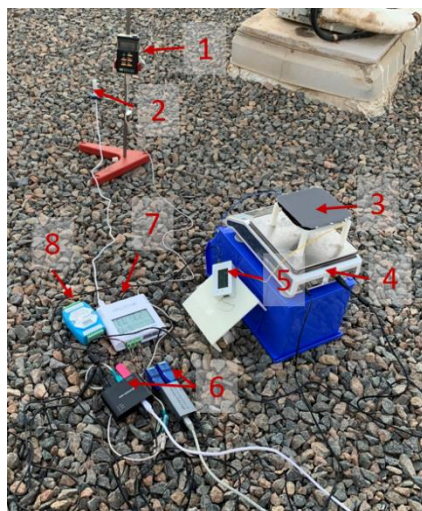
The accumulative electricity generation was shown in Supplementary Figure 13f. Considering the difference in solar irradiance between August 14 and August 15, an efficiency enhancement of ~19% was calculated. This value is actually slightly higher than the one observed in the lab condition presumably due to strong wind-field-facilitated evaporation and heat dissipation in the field condition. Further, the replacement of hydrogel in the middle of the test further enhanced the cooling performance.



Supplementary Figure 13. (a) Sunlight strength, (b) overall solar irradiance, (c) relative humidity and (d) ambient temperature of August 14 and August 15, 2019. (e) Power and surface temperature of PV panel. (f) Accumulated electricity generated on August 14 and August 15.

Outdoor field test in winter

The experimental setup of the outdoor test conducted in winter was further modified to enable in-situ and better monitoring of the weight change of hydrogel, PV panel temperature, ambient condition, and PV performance/properties (Supplementary Figure 14). Similarly, the PV panel was also horizontally placed on the roof top without any tilting angle. In comparison with the summer setup, an electrical balance and a thermal couple were used to monitor the weigh change of hydrogel and the temperature of the PV panel. A digital humidity and temperature meter was used to monitor the ambient condition.



Supplementary Figure 14. Experimental setup of PV panel cooling test in outdoor condition in early-December, 2019. 1-solar meter; 2-humidity and temperature sensor; 3-PV panel placed on the holder frame and attached with hydrogel cooling layer; 4-electrical balance; 5-coulomb meter; 6-communication hub; 7-humidity and temperature meter; 8-thermal couple module, the wired-thermal couple was attached on the backside of PV panel above the hydrogel cooling layer.

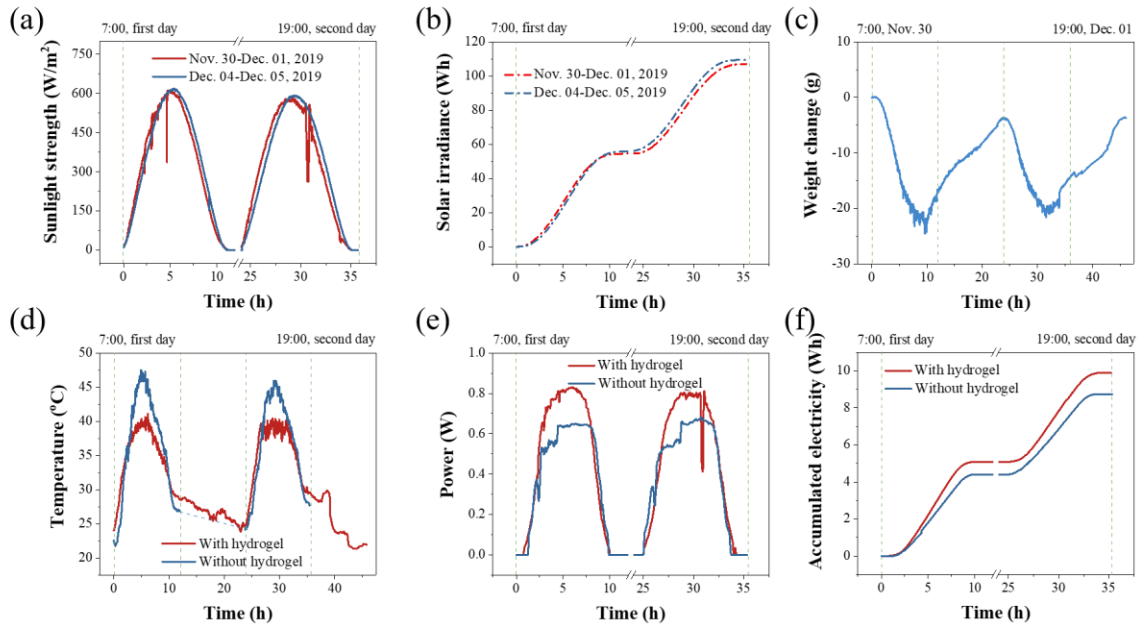
The outdoor test was conducted for two days for each mode for comparison, i.e., the PV panel with hydrogel cooling layer was examined from November 30 to December 2, 2019, and the PV panel without the cooling layer was tested from December 4 to December 5, 2019. The sunlight strength and the overall solar irradiance for the two different working conditions were recorded by a solar meter and plotted in Supplementary Figure 15a and b. As can be seen, the sunlight strength and the overall solar irradiance of the two working conditions (i.e. November 30 to December 1, 2019, and December 4 to December 5, 2019) are quite close.

For the cooling mode, the properties and the pre-treatment method of hydrogel were the same as the one in the summer test. The original weight (i.e. the weight of polyacrylamide, CaCl_2 , and residual water) was measured to be 96 g. The hydrogel was attached on the backside of the PV panel and placed on top of the holder frame overnight, and the electrical balance was zeroed at 7:00 am on November 30 when the experiment was initiated. The weight change curve of the two full-desorption-sorption cycles of the hydrogel was also observed and plotted (Supplementary Figure 15c). As can be seen, the weight loss of hydrogel due to water evaporation/desorption was stopped at around 17:00 for both days, which was because the sunlight strength at this time was too weak to generate sufficient amount of heat to maintain water evaporation/desorption. The actual working hours of cooling layer was about 10 hours. From ~17:00 to ~8:00 the day after (i.e. ~15 hours), the weight of the hydrogel recovered, indicating water vapor sorption took place on the hydrogel. The amount of water released/captured by the hydrogel (i.e., the lost weight and the recovered weight) was highly dependent on sunlight strength and the weather condition of the surrounding ambient (Supplementary Figure 16a and b). Thus, the weight change curve of November 30 and December 1 displayed a similar trend but different values.

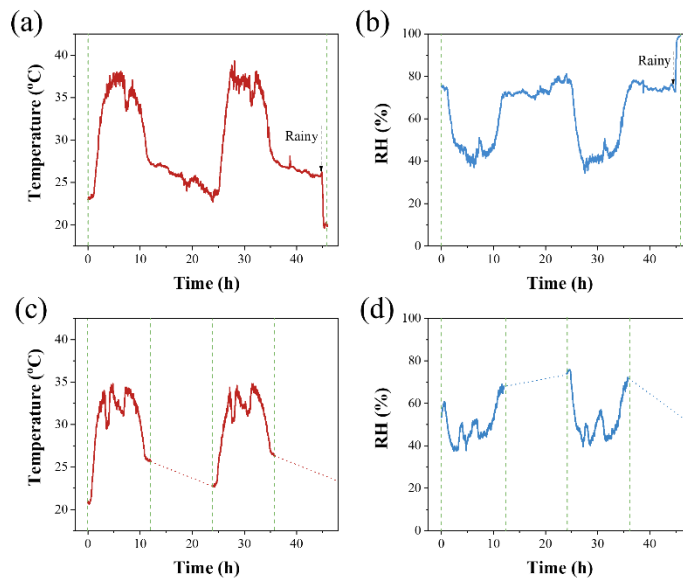
Meanwhile, the amount of evaporated water and recovered water of hydrogel during the winter test was lower than that of the summer test. This phenomenon can be attributed to the weakened water evaporation due to the weakened sunlight strength and lowered ambient temperature in winter. To further demonstrate the water sorption capability of the hydrogel, the sorption test was further extended to the morning of December 2. It has to be mentioned that due to the predicted rainfall on December 2, a curved aluminum rain shelter was installed on top of the electrical balance at ~20:00 on December 1, and thus the weight loss curve after this time showed a smoother appearance due to the reduced airflow turbulence. The weight change curve observed from the real-outdoor condition indicates the choice of the hydrogel thickness and the hydrogel water vapor sorption/desorption properties were suitable for the practical applications.

The cooling performance (i.e. the temperature of PV panel) of PV panel with and without hydrogel is compared in Supplementary Figure 15d. As can be seen, a peak value of ~8 °C of temperature difference can be observed when the hydrogel cooling layer was employed. This value is lower than the one observed in summer (i.e., 10.6 °C) due to the attenuated sunlight strength in winter and the lowered ambient temperature. The power of the PV panel and the accumulated electricity generation during the tests are compared in Supplementary Figure 17e and f. For most of the time, the power of PV panel with cooling layer attached shows a higher value than that of without cooling layer.

However, the different weather condition and the sunlight irradiation still led to another phenomenon—in some time schemes (i.e., before 9:00 or after 17:00) within a day during the winter test, the batch with cooling layer attached even showed a higher temperature than that of the PV panel without cooling layer. Fortunately, the temperature rise was insignificant. The accumulated electricity generation under two different conditions are calculated to be 9.89 and 8.74 Wh for PV with and without the cooling layer, respectively. Considering the difference in solar irradiation, the same PV panel with the cooling layer could still generate ~13.5% more electricity even worked in a lower ambient temperature. Even though this value is lower than the one observed in summer (i.e., 19%), the performance enhancement is still considerable.



Supplementary Figure 15. (a) Sunlight strength curve of November 30, December 01, December 4, and December 5, 2019. (b) Overall solar irradiance of the two individual outdoor test. (c) Weight change curve of the hydrogel cooling layer during the test. (d) PV panel temperature during the test. (e) The power of PV panel. (f) Accumulated electricity generated during the test observed from the two modes.



Supplementary Figure 16. Temperature and relative humidity of (a)-(b) November 30-December 2, (c)-(d) December 4-5. For the outdoor test without hydrogel cooling layer, we only monitored the ambient condition within the test period.

As a brief conclusion, the two outdoor test conducted in different seasons successfully demonstrate the feasibility of the concept of utilizing atmospheric water as coolant to cool down the PV panel. The tests showed very satisfactory performances in both summer and winter, with the former being better than the latter.

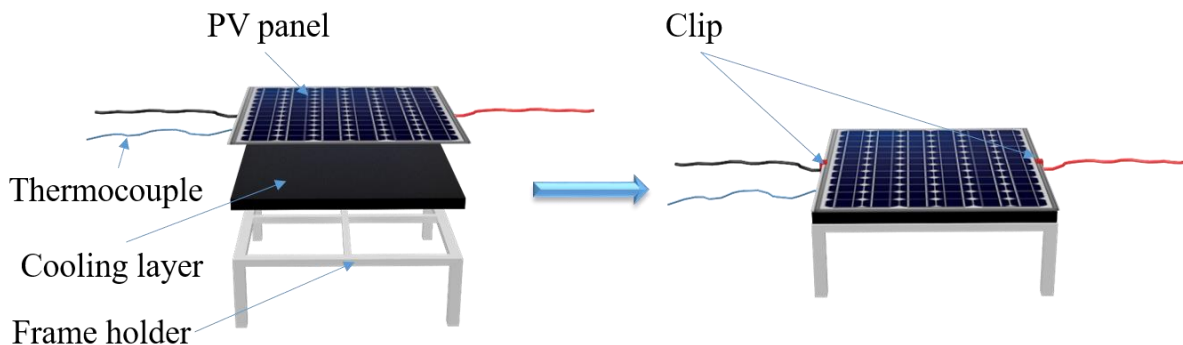
In addition, we further performed 7 cycles outdoor field tests which confirm performance recyclability of the hydrogel cooling layers, including water sorption and desorption capacities, cooling performances, along with PV electricity generation performance. The outdoor PV-cooling recyclability test is shown in Supplementary Figure 17.

The test was performed between December 27, 2019 at 00:00 and January 2, 2020 at 24:00 (GMT+3) in KAUST campus, Saudi Arabia. The sunlight strength, ambient condition, weight change of cooling layer, temperature and power of PV panel during operation, and the daily electricity generation were recorded.

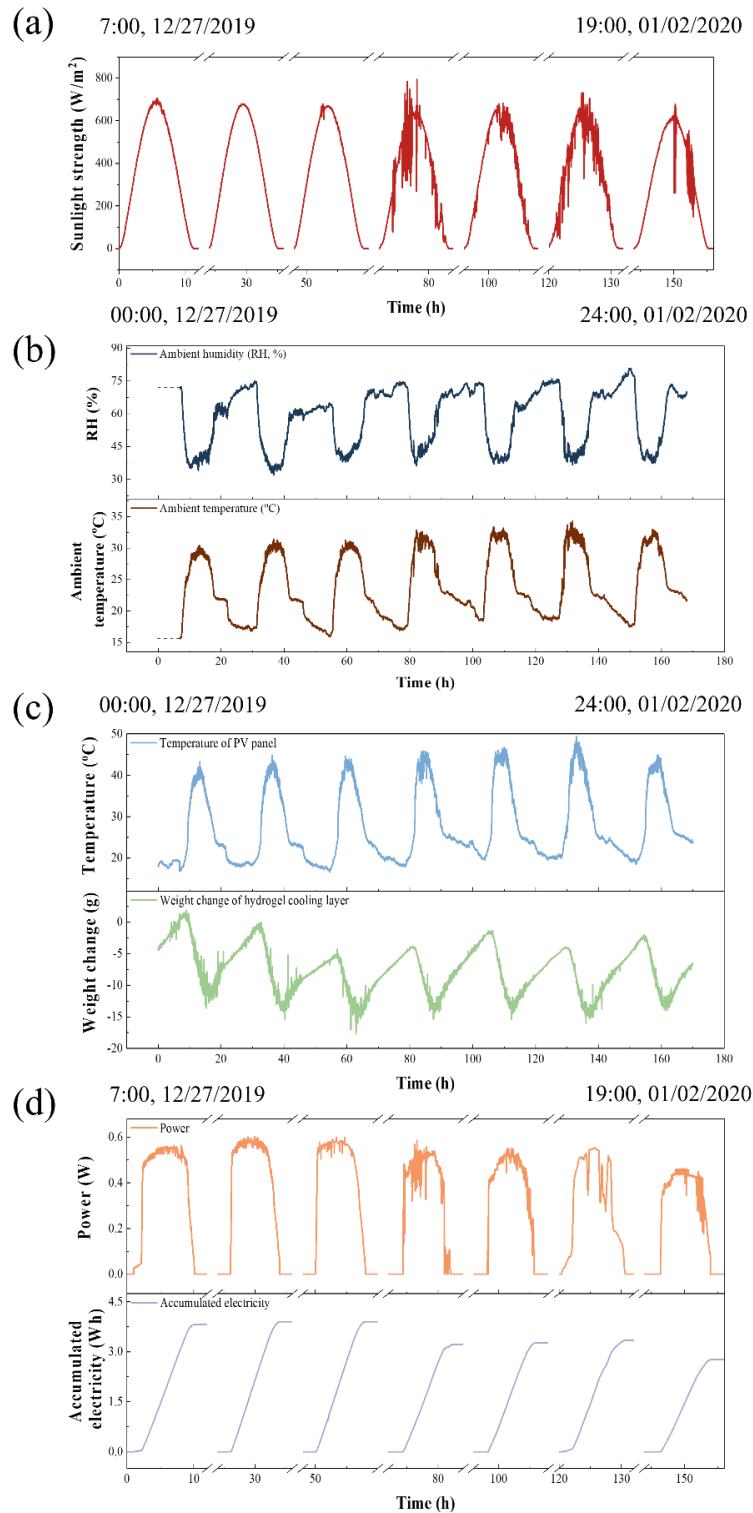
The variations of solar irradiation, relative humidity and ambient temperature are presented in Supplementary Figure 18a and b. As can be seen from the solar irradiation curve (Supplementary Figure 18a), the weather of day 4 to day 7 was a bit cloudy with fluctuation on solar irradiation intensity.

The temperature curve of PV panel is displayed in Supplementary Figure 18c. As can be seen, the cooling layer successfully maintained the temperature difference between PV panel and the ambient within 5-10 °C throughout the test days. The weight change curve of the hydrogel cooling layer (Supplementary Figure 18c) demonstrates the water removal pattern is repeatable, with variation largely due to the daily weather conditions. As can be seen from Supplementary Figure 18, the working capacities of the hydrogel and PV panel are highly depended on the outdoor weather conditions.

All of these results successfully demonstrate both structural and performance stability of the cooling layer design.



Supplementary Figure 17. Schematic of outdoor test PV-hydrogel system.



Supplementary Figure 18. (a) Solar irradiation during stability test. The cloudy weather of day 4 to day 7 is reflected in the sunlight strength curve. (b) The ambient condition during the stability test. (c) The temperature of PV panel and the weight change curve of the hydrogel cooling layer.

(d) The power of PV panel during operation and the accumulated electricity generated in daily base.

Supplementary Table 3. Parameters of simulated daylight test.

Light strength (W/m ²)	Cumulative illumination time (hours)	Simulated time scale
400	1	7:00-8:00
600	2	8:00-9:00
800	3	9:00-10:00
950	4	10:00-11:00
1040	5	11:00-12:00
1060	6	12:00-13:00
1030	7	13:00-14:00
940	8	14:00-15:00
800	9	15:00-16:00
600	10	16:00-17:00
400	11	17:00-18:00

Supplementary note 3. Recent publications on AWH cooling concept on other journals

During the review and revision process of this manuscript, it was noted that three papers on similar concept were published on other journals.¹¹⁻¹³ These three publications explored atmospheric-water-harvesting for cooling in three different scenarios, electronic device cooling, semiconductor cooling, and actuator cooling.

This work was submitted to Nature Sustainability for consideration on January 11, 2019, which was earlier than the submission dates of these three works (see below).

- Wang, C. *et al.* A thermal management strategy for electronic devices based on moisture sorption-desorption processes. *Joule* **4**, 435-447 (2020). (submission date: 18 August 2019)
- Pu, S. *et al.* Promoting energy efficiency via a self-adaptive evaporative cooling hydrogel. *Adv. Mater.*, 1907307 (2020). DOI: 10.1002/adma.201907307. (submission date: 7 November 2019)
- Mishra, A., K. *et al.* Autonomic perspiration in 3D-printed hydrogel actuators. *Sci. Robot.* **5**, eaaz3918 (2020). (Submission date: 5 September 2019)

In addition, we confirm that none of the authors of this work was involved in reviewing any of these three during their review processes in any journal. Therefore, it is safe to say that this work independently developed AWG-assisted cooling concept and provided its proof-of-concept.

These publications altogether demonstrate that AWH cooling is emerging as a new cooling paradigm, offers a broad range of benefits and represents a solid force toward global sustainability.

References

1. <https://www.oxy.com/OurBusinesses/Chemicals/Products/Documents/CalciumChloride/173-01791.pdf>
2. Rammelberg, H. U., Schmidt, T., and Ruck, W. Hydration and Dehydration of Salt Hydrates and Hydroxides for Thermal Energy Storage-Kinetics and Energy Release. *Energy Procedia* **30**, 362 – 369 (2012).
3. Baumgartner, M. and Bakker, R. J., CaCl₂-Hydrate Nucleation in Synthetic Fluid Inclusions. *Chem. Geol.* **265** 335–344 (2009).
4. Smith, R. L. Predicting Evaporation Rates and Times for Spills of Chemical Mixtures. *Ann. Occup. Hyg.* **45** 437-445 (2001).
5. Chiavazzo, E., Morciano, M., Viglino, F. et al. Passive solar high-yield seawater desalination by modular and low-cost distillation. *Nat Sustain* **1**, 763–772 (2018).
6. Zhang, L. Z. Mass Diffusion in a Hydrophobic Membrane Humidification/Dehumidification Process: the Effects of Membrane Characteristics. *Sep. Sci. Technol.* **41** (2006) 1565-1582.
7. https://www.engineersedge.com/physics/viscosity_of_air_dynamic_and_kinematic_14483.htm
8. Hall, J. R., Wishaw, B. F., and Stokes, R. H. The Diffusion Coefficients of Calcium Chloride and Ammonium Chloride in Concentrated Aqueous Solutions at 25 °C. *J. Am. Chem. Soc.* **75** 1556-1560 (1953).
9. Conde, M. R. Properties of Aqueous Solutions of Lithium and Calcium Chlorides: Formulations for Use in Air Conditioning Equipment Design. *Int. J. Therm. Sci.* **43** 367–382 (2004).
10. Li, R. Zhang, L., Shi, L., and Wang, P. MXene Ti₃C₂: An Effective 2D Light-to-Heat Conversion Material. *ACS Nano* **11**, 3752-3759 (2017).
11. Wang, C. *et al.* A thermal management strategy for electronic devices based on moisture sorption-desorption processes. *Joule* **4**, 435-447 (2020).
12. Pu, S. *et al.* Promoting energy efficiency via a self-adaptive evaporative cooling hydrogel. *Adv. Mater.*, 1907307 (2020). DOI: 10.1002/adma.201907307.
13. Mishra, A., K. *et al.* Autonomic perspiration in 3D-printed hydrogel actuators. *Sci. Robot.* **5**, eaaz3918 (2020).